Available online at www.sciencedirect.com
ScienceDirect
International Journal of Solids and Structures 44 (2007) 6340–6359
INTERNATIONAL JOURNAL OF SOLIDS AND STRUCTURES
www.elsevier.com/locate/ijsolstr

A unified definition for stress intensity factors of interface corners and cracks

Chyanbin Hwu *, T.L. Kuo

Institute of Aeronautics and Astronautics, National Cheng Kung University, Tainan, Taiwan, ROC

Received 24 April 2006; received in revised form 31 January 2007
Available online 25 February 2007

Abstract

Based upon linear fracture mechanics, it is well known that the singular order of stresses near the crack tip in homogeneous materials is a constant value $-1/2$, which is nothing to do with the material properties. For the interface cracks between two dissimilar materials, the near tip stresses are oscillatory due to the order of singularity being $-1/2 \pm i\varepsilon$ and $-1/2$. The oscillation index ε is a constant related to the elastic properties of both materials. While for the general interface corners, their singular orders depend on the corner angle as well as the elastic properties of the materials. Owing to the difference of the singular orders of homogeneous cracks, interface cracks and interface corners, their associated stress intensity factors are usually defined separately and even not compatibly. Since homogenous cracks and interface cracks are just special cases of interface corners, in order to build a direct connection among them a unified definition for their stress intensity factors is proposed in this paper. Based upon the analytical solutions obtained previously for the multibonded anisotropic wedges, the near tip solutions for the general interface corners have been divided into five different categories depending on whether the singular order is distinct or repeated, real or complex. To provide a stable and efficient computing approach for the general mixed-mode stress intensity factors, the path-independent *H*-integral based on reciprocal theorem of Betti and Rayleigh is established in this paper. The complementary solutions needed for calculation of *H*-integral are also provided in this paper. To illustrate our results, several different kinds of examples are shown such as cracks in homogenous isotropic or anisotropic materials, central or edge notches in isotropic materials, interface cracks and interface corners between two dissimilar materials.

Keywords: Stress intensity factor; Singular orders; Interface corners; Interface cracks; Multibonded wedge; Path-independent integrals; Anisotropic elasticity; Stroh formalism

1. Introduction

Electric devices are composed of many different parts. Because each part may be made from different materials and may have different shapes, it is very possible that many interface corners exist in several local fields of

* Corresponding author. Tel.: +886 6 2757575x63662; fax: +886 2389940.
E-mail address: CHwu@mail.ncku.edu.tw (C. Hwu).

0020-7683/$ - see front matter
doi:10.1016/j.ijsolstr.2007.02.031

an electric device. Due to the mismatch of thermal or elastic properties, stress singularity usually occurs near the interface corners, which may initiate failure of structures. Therefore, it is important to design a proper joint shape to prevent the failure initiation and propagation. The *singular order* of stresses near the interface corners is a good index for the understanding of failure initiation. However, in engineering applications one usually feels only the knowledge of singular orders is not enough for the prediction of failure initiation. The most apparent examples are homogeneous cracks whose singular order is $-1/2$ which is a constant value and is nothing to do with the surrounding environment and outside loading of cracks. These influential factors are reflected through another important parameter – *stress intensity factor*. Therefore, in addition to the singular orders one is always interested to know their associated stress intensity factors of interface corners.

Although several detailed studies have been done about the determination of the associated singular orders and stress intensity factors for interface corners, very few failure criteria were successfully established based upon these parameters. Even the cracks in homogeneous media or the cracks lying along the interface between dissimilar materials are the special cases of the interface corners, the definitions of stress intensity factors proposed in the literature are usually not consistent with that of cracks. Therefore, to have a universal failure criterion for the homogeneous cracks, interface cracks and interface corners, a unified definition for the stress intensity factors is indispensable. In the literature the stress intensity factors of interface corners are usually defined by the way similar to the homogeneous cracks, e.g., (Sinclair et al., 1984; Dunn et al., 1997), which may encounter trouble when the stress distributions near the interface corners exhibit the oscillatory characteristics like the interface cracks discussed in (Rice, 1988; Wu, 1990; Suo, 1990; Gao et al., 1992; Hwu, 1993). Thus, even for the interface cracks some definitions of their stress intensity factors proposed in the literature are not compatible with the conventional definitions for homogeneous cracks. To build a direct connection among the homogeneous cracks, interface cracks and interface corners, in this paper a unified definition for the stress intensity factors is proposed.

According to the experience of crack problems, finding a stable and accurate approach to calculate the stress intensity factors is also important. By the definition of the stress intensity factors proposed in this paper, to calculate their values we need to know the stresses near the tip of interface corners. By employing the Stroh formalism for anisotropic elasticity (Ting, 1996), the near tip solutions for elastic composite wedges have been obtained analytically (Hwu et al., 2003). Moreover, consideration of the thermal effects, the solutions for the temperature, heat flux, displacement and stress in the field near the apex of multibonded anisotropic wedges are also obtained (Hwu and Lee, 2004). Based upon the analytical solutions obtained from (Hwu and Lee, 2004), in this paper the near tip solutions for the general interface corners are divided into five different categories depending on whether the singular order is distinct or repeated, real or complex. However, due to the singular and possibly oscillatory behaviors of the near tip solutions, it is not easy to get convergent values for the stress intensity factors directly from the definition. To overcome this problem, a path-independent H-integral (Stern et al., 1976; Sinclair et al., 1984; Labossiere and Dunn, 1999) is employed to compute the possibly mixed-mode stress intensity factors, in which the complementary solutions needed for calculation are derived in this paper. By using the H-integral, the complexity of stresses around the tip of interface corners can then be avoided.

2. Near tip solutions for multibonded anisotropic wedges

To study the singular behavior of interface corners and to provide a proper definition for their associated stress intensity factors, like the concept of fracture mechanics it is important to know the near tip solutions. By employing Stroh formalism for anisotropic elasticity, the near tip solutions for multibonded anisotropic wedges have been obtained as (Hwu et al., 2003; Hwu and Lee, 2004)

$$\mathbf{w}_k(r,\theta) = r^{\lambda}\mathbf{E}_k^*(\theta)\mathbf{K}_{k-1}\mathbf{w}_0, \quad k = 1,2,3,\ldots,n, \tag{2.1}$$

in which (r,θ) is the polar coordinate with origin located on the wedge apex; $\mathbf{w}_k(r,\theta)$, $k = 1, 2, \ldots, n$, is a 6×1 vector composed of the displacements and stress functions of the kth wedge; $\mathbf{w}_0$ is a 6×1 coefficient vector related to $\mathbf{w}_1(r,\theta_0)$ by $\mathbf{w}_1(r,\theta_0) = r^{\lambda}\mathbf{w}_0$; $\mathbf{E}_k^*(\theta)$ and $\mathbf{K}_{k-1}$ are 6×6 matrices related to the material properties of the wedges. They are defined by (Note that for simplicity the symbols $1-\delta$ and $(\mathbf{K}_e)_{k-1}$ used in (Hwu and Lee, 2004) has been replaced by λ and $\mathbf{K}_{k-1}$)

$$
\begin{aligned}
&\mathbf{w}_0 = \left\{ \begin{array}{c} \mathbf{u}_0 \\ \boldsymbol{\phi}_0 \end{array} \right\}, \quad \mathbf{w}_k(r,\theta) = \left\{ \begin{array}{c} \mathbf{u}_k(r,\theta) \\ \boldsymbol{\phi}_k(r,\theta) \end{array} \right\}, \\
&\mathbf{u}_k(r,\theta) = \left\{ \begin{array}{c} u_1(r,\theta) \\ u_2(r,\theta) \\ u_3(r,\theta) \end{array} \right\}_k, \quad \boldsymbol{\phi}_k(r,\theta) = \left\{ \begin{array}{c} \phi_1(r,\theta) \\ \phi_2(r,\theta) \\ \phi_3(r,\theta) \end{array} \right\}_k, \\
&\mathbf{E}_k^*(\theta) = \hat{\mathbf{N}}_k^{\lambda}(\theta,\theta_{k-1}), \quad k = 1,2,3,\ldots,n, \\
&\mathbf{K}_{k-1} = \left\{ \begin{array}{ll} \mathbf{I}, & k = 1, \\ \prod\limits_{i=1}^{k-1} \mathbf{E}_{k-i} = \mathbf{E}_{k-1}\mathbf{E}_{k-2}\ldots\mathbf{E}_1, & k = 2,3,\ldots,n, \end{array} \right.
\end{aligned}
\tag{2.2}
$$

in which $\mathbf{E}_k = \mathbf{E}_k^*(\theta_k) = \hat{\mathbf{N}}_k^{\lambda}(\theta_k,\theta_{k-1})$, and θ_k, θ_{k-1} are the angular location of the two sides of the kth wedge (Fig. 1(a)). u_i, $i = 1, 2, 3$, are the displacements in x_i-directions, ϕ_i, $i = 1, 2, 3$, are the stress functions related to the Cartesian stress components σ_{ij} and surface traction vector $\mathbf{t}$ by

$$\sigma_{i1} = -\phi_{i,2}, \quad \sigma_{i2} = \phi_{i,1}, \tag{2.3a}$$

$$\mathbf{t} = \partial\boldsymbol{\phi}/\partial s, \tag{2.3b}$$

where s is the arc length measured along the curved boundary such that when one faces the direction of increasing s the material lies on the right side. From (2.3b), we have $\mathbf{t} = \boldsymbol{\phi}_{,r}$ for a radial line surface and $\mathbf{t} = \boldsymbol{\phi}_{,\theta}/r$ for a circular surface, and hence, the stresses in polar coordinate can also be calculated from the stress functions $\boldsymbol{\phi}$ by

$$
\begin{aligned}
&\sigma_{\theta\theta} = \mathbf{m}^{\mathrm{T}}\boldsymbol{\phi}_{,r}, \quad \sigma_{rr} = -\mathbf{n}^{\mathrm{T}}\boldsymbol{\phi}_{,\theta}/r, \quad \sigma_{r\theta} = \mathbf{n}^{\mathrm{T}}\boldsymbol{\phi}_{,r} = -\mathbf{m}^{\mathrm{T}}\boldsymbol{\phi}_{,\theta}/r, \\
&\sigma_{\theta z} = (\boldsymbol{\phi}_{,r})_z, \quad \sigma_{rz} = -(\boldsymbol{\phi}_{,\theta})_z/r,
\end{aligned}
\tag{2.4a}
$$

where

$$\mathbf{n}^{\mathrm{T}} = (\cos\theta \quad \sin\theta \quad 0), \quad \mathbf{m}^{\mathrm{T}} = (-\sin\theta \quad \cos\theta \quad 0). \tag{2.4b}$$

In (2.2), $\hat{\mathbf{N}}$ is a 6×6 matrix related to the Stroh fundamental matrix $\mathbf{N}$ (Ting, 1996) by

$$\hat{\mathbf{N}}_k^{\lambda}(\theta,\theta_{k-1}) = [\cos(\theta-\theta_{k-1})\mathbf{I} + \sin(\theta-\theta_{k-1})\mathbf{N}_k(\theta_{k-1})]^{\lambda}, \tag{2.5}$$

in which $\mathbf{I}$ is a 6×6 identity matrix. Because in general λ is not an integer, to calculate the λ power of $\hat{\mathbf{N}}$ one usually use the transformation through the eigenvalues and eigenvectors of $\mathbf{N}$. By this way, it has been proved that (Hwu et al., 2003)

$$\hat{\mathbf{N}}_k^{\lambda}(\theta,\theta_{k-1}) = \begin{bmatrix} \mathbf{A}_k & \overline{\mathbf{A}}_k \\ \mathbf{B}_k & \overline{\mathbf{B}}_k \end{bmatrix} \begin{bmatrix} \langle \hat{\mu}_*^{\lambda}(\theta,\theta_{k-1})\rangle & \mathbf{0} \\ \mathbf{0} & \langle \overline{\hat{\mu}}_*^{\lambda}(\theta,\theta_{k-1})\rangle \end{bmatrix} \begin{bmatrix} \mathbf{B}_k^{\mathrm{T}} & \mathbf{A}_k^{\mathrm{T}} \\ \overline{\mathbf{B}}_k^{\mathrm{T}} & \overline{\mathbf{A}}_k^{\mathrm{T}} \end{bmatrix}, \tag{2.6}$$

in which the overbar denotes the complex conjugate; the angular bracket $\langle\rangle$ stands for a diagonal matrix in which each component is varied according to the subscript $*$, e.g., $\langle z_*\rangle = \mathrm{diag}.[z_1,z_2,z_3]$; the superscript T denotes the transpose of a matrix. $\mathbf{A}$ and $\mathbf{B}$ are two 3×3 material eigenvector matrices and $\hat{\mu}_*^{\lambda}(\theta,\theta_{k-1})$ is related to the material eigenvalues μ_* by

$$\hat{\mu}_*^{\lambda}(\theta,\theta_{k-1}) = [\cos(\theta-\theta_{k-1}) + \sin(\theta-\theta_{k-1})\mu_*(\theta_{k-1})]^{\lambda}, \quad * = 1,2,3, \tag{2.7a}$$

and

$$\mu_*(\theta_{k-1}) = \frac{\mu_*\cos\theta_{k-1} - \sin\theta_{k-1}}{\mu_*\sin\theta_{k-1} + \cos\theta_{k-1}}. \tag{2.7b}$$

In the above, $\lambda - 1$ is the order of the stress singularity which will be influenced by the wedge configurations (n wedge angles) and properties ($21n$ elastic constants), and the boundary conditions of wedge surfaces. For free–free wedge $\boldsymbol{\phi}_1(r,\theta_0) = \boldsymbol{\phi}_n(r,\theta_n) = \mathbf{0}$, detailed derivation will lead to (Hwu and Lee, 2004)

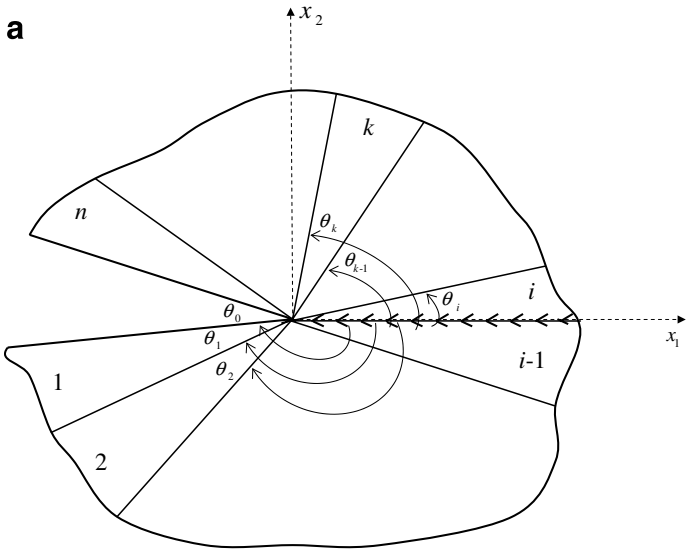

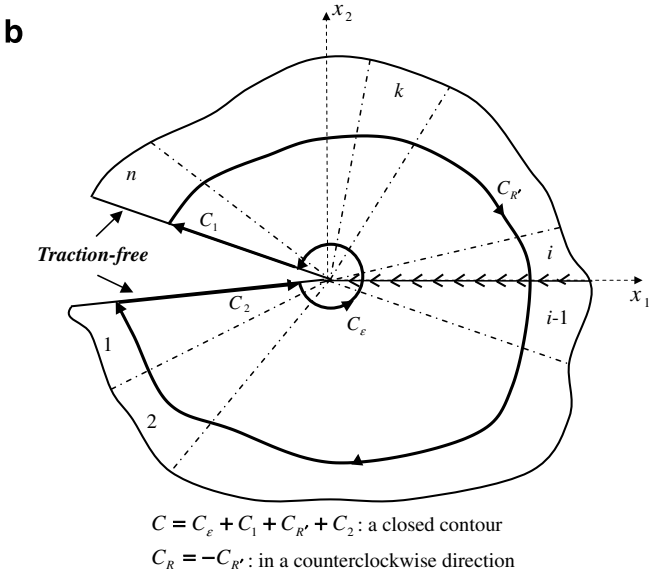

Fig. 1. (a) n-Multibonded anisotropic wedges. (b) Schematic diagram of H-integral contour.

$$\boldsymbol{\phi}_0 = \mathbf{0}, \quad \mathbf{K}^{(3)}\mathbf{u}_0 = \mathbf{0}, \tag{2.8a}$$

where $\mathbf{K}^{(3)}$ is one of the submatrices of $\mathbf{K}$ which is related to $\mathbf{E}_k$ by

$$\mathbf{K} = \prod_{k=1}^{n} \mathbf{E}_{n-k+1} = \mathbf{E}_n \mathbf{E}_{n-1} \ldots \mathbf{E}_1, \quad \mathbf{K} = \begin{bmatrix} \mathbf{K}^{(1)} & \mathbf{K}^{(2)} \\ \mathbf{K}^{(3)} & \mathbf{K}^{(4)} \end{bmatrix}. \tag{2.8b}$$

Nontrivial solution of $\mathbf{u}_0$ exists only when the determinant of $\mathbf{K}^{(3)}$ is equal to zero, i.e., $\|\mathbf{K}^{(3)}\| = 0$, which will give us the singular order $\lambda - 1$. After obtaining the singular orders that may be real or complex, distinct or repeated, the nonzero values of $\mathbf{u}_0$ can then be calculated through $(2.8a)_2$. With λ and $\mathbf{w}_0 = (\mathbf{u}_0\ \mathbf{0})^{\mathrm{T}}$ determined, the near tip solution (2.1) can now be expanded as

$$\begin{aligned}\mathbf{u}_k(r,\theta) &= r^{\lambda}\left\{\mathbf{E}_k^{*(1)}(\theta)\mathbf{K}_{k-1}^{(1)} + \mathbf{E}_k^{*(2)}(\theta)\mathbf{K}_{k-1}^{(3)}\right\}\mathbf{u}_0,\\ \boldsymbol{\phi}_k(r,\theta) &= r^{\lambda}\left\{\mathbf{E}_k^{*(3)}(\theta)\mathbf{K}_{k-1}^{(1)} + \mathbf{E}_k^{*(4)}(\theta)\mathbf{K}_{k-1}^{(3)}\right\}\mathbf{u}_0,\end{aligned} \tag{2.9a}$$

where $\mathbf{E}_k^{*(i)}(\theta)$ and $\mathbf{K}_{k-1}^{(i)}$ are the submatrices of $\mathbf{E}_k^{*}(\theta)$ and $\mathbf{K}_{k-1}$ defined by

$$\mathbf{E}_k^{*}(\theta) = \begin{bmatrix}\mathbf{E}_k^{*(1)}(\theta) & \mathbf{E}_k^{*(2)}(\theta)\\ \mathbf{E}_k^{*(3)}(\theta) & \mathbf{E}_k^{*(4)}(\theta)\end{bmatrix}, \quad \mathbf{K}_{k-1} = \begin{bmatrix}\mathbf{K}_{k-1}^{(1)} & \mathbf{K}_{k-1}^{(2)}\\ \mathbf{K}_{k-1}^{(3)} & \mathbf{K}_{k-1}^{(4)}\end{bmatrix}. \tag{2.9b}$$

From $(2.8a)_2$ and the definitions given in (2.2) and (2.5)–(2.7), we see that the singular orders are totally determined through the material properties and configurations of all wedges. Since we consider the singular fields and the strain energy cannot be unbounded, only the values located in the range of $0 < \mathrm{Re}(\lambda) < 1$ are considered in this paper. If more than one λ locate in this range, we select the one whose real part is minimum as λ_c, i.e., the one with the most critical singular order $\lambda_c - 1$. If λ_c is a complex number, it has been proved that its conjugate $\overline{\lambda}_c$ is also a root of $\|\mathbf{K}^{(3)}\| = 0$ (Hwu et al., 2003).

When $r \to 0$, i.e., the near tip field, the terms associated with λ_c will dominate the stress behavior. Neglecting all the other singular and nonsingular terms, and expanding the near tip solution (2.1) for the terms associated with λ_c, we may express the displacement and stress function vectors in terms of the eigenvector $\mathbf{u}_0$ obtained from $(2.8a)_2$. However, an eigenvalue λ_c may correspond several linearly independent eigenvectors $\mathbf{u}_0$. If λ_c is a nonrepeated root, only one arbitrary scalar is needed to describe $\mathbf{u}_0$. When λ_c is a double root, two arbitrary scalars are needed. While for a triple root λ_c, three arbitrary scalars are needed. If λ_c is complex, the arbitrary scalar associated with $\mathbf{u}_0$ is also complex which contains two real scalars. With the above understanding, the near tip solutions (2.9a) may now be rewritten as

Case 1: λ_c is distinct and real, $\lambda_c = \lambda_R$,

$$\begin{aligned}\mathbf{u}(r,\theta) &= cr^{\lambda_R}\mathbf{p}(\theta),\\ \boldsymbol{\phi}(r,\theta) &= cr^{\lambda_R}\mathbf{q}(\theta).\end{aligned} \tag{2.10a}$$

Case 2: λ_c is double and real, $\lambda_c = \lambda_R$,

$$\begin{aligned}\mathbf{u}(r,\theta) &= r^{\lambda_R}\{c_1\mathbf{p}_1(\theta) + c_2\mathbf{p}_2(\theta)\},\\ \boldsymbol{\phi}(r,\theta) &= r^{\lambda_R}\{c_1\mathbf{q}_1(\theta) + c_2\mathbf{q}_2(\theta)\}.\end{aligned} \tag{2.10b}$$

Case 3: λ_c is triple and real, $\lambda_c = \lambda_R$,

$$\begin{aligned}\mathbf{u}(r,\theta) &= r^{\lambda_R}\{c_1\mathbf{p}_1(\theta) + c_2\mathbf{p}_2(\theta) + c_3\mathbf{p}_3(\theta)\},\\ \boldsymbol{\phi}(r,\theta) &= r^{\lambda_R}\{c_1\mathbf{q}_1(\theta) + c_2\mathbf{q}_2(\theta) + c_3\mathbf{q}_3(\theta)\}.\end{aligned} \tag{2.10c}$$

Case 4: λ_c is distinct and complex, $\lambda_c = \lambda_R \pm i\varepsilon$,

$$\begin{aligned}\mathbf{u}(r,\theta) &= r^{\lambda_R}\left\{cr^{i\varepsilon}\mathbf{p}(\theta) + \bar{c}r^{-i\varepsilon}\overline{\mathbf{p}(\theta)}\right\},\\ \boldsymbol{\phi}(r,\theta) &= r^{\lambda_R}\left\{cr^{i\varepsilon}\mathbf{q}(\theta) + \bar{c}r^{-i\varepsilon}\overline{\mathbf{q}(\theta)}\right\}.\end{aligned} \tag{2.10d}$$

Case 5: one is real λ_R and the others are complex $\lambda_R \pm i\varepsilon$,

$$\begin{aligned}\mathbf{u}(r,\theta) &= r^{\lambda_R}\left\{cr^{i\varepsilon}\mathbf{p}_1(\theta) + \bar{c}r^{-i\varepsilon}\overline{\mathbf{p}_1(\theta)} + c_3\mathbf{p}_3(\theta)\right\},\\ \boldsymbol{\phi}(r,\theta) &= r^{\lambda_R}\left\{cr^{i\varepsilon}\mathbf{q}_1(\theta) + \bar{c}r^{-i\varepsilon}\overline{\mathbf{q}_1(\theta)} + c_3\mathbf{q}_3(\theta)\right\}.\end{aligned} \tag{2.10e}$$

In the above, $\mathbf{p}(\theta)$ and $\mathbf{q}(\theta)$ (or $\mathbf{p}_i(\theta)$ and $\mathbf{q}_i(\theta)$, $i = 1, 2, 3$) are functions related to $\mathbf{E}_k^{*(i)}(\theta)$, $\mathbf{K}_{k-1}^{(i)}$ and $\mathbf{u}_0$ in which the number of arbitrary scalars is dependent on the multiplicity of λ_c. Note that the solutions shown in (2.10a–e) are valid for any wedge of the multibonded wedges, and hence from now on unless special notification is needed the subscript k denoting the wedge has been neglected for simplicity.

3. A unified definition for stress intensity factors

It is known that a semi-infinite crack in homogeneous materials can be represented by letting $\theta_0 = -\pi$ and $\theta_1 = \pi$ for a single wedge. Moreover, an interface crack can be represented by a bi-wedge with $\theta_0 = -\pi$, $\theta_1 = 0$ and $\theta_2 = \pi$. These two important special cases indicate that to propose a proper definition for the stress intensity factors of interface corners, it is better to review the corresponding definition for the crack problems.

A conventional definition for the stress intensity factors $\mathbf{k}$ of a crack in homogeneous media is (Broek, 1974)

$$\mathbf{k} = \begin{Bmatrix} K_{II} \\ K_I \\ K_{III} \end{Bmatrix} = \lim_{\substack{r\to 0 \\ \theta=0}} \sqrt{2\pi r} \begin{Bmatrix} \sigma_{r\theta} \\ \sigma_{\theta\theta} \\ \sigma_{\theta z} \end{Bmatrix} = \lim_{\substack{r\to 0 \\ \theta=0}} \sqrt{2\pi r}\boldsymbol{\phi}_{,r}, \tag{3.1}$$

in which the third equality of (3.1) comes from the relations given in (2.4); $\theta = 0$ is a line along the crack. Due to the oscillatory behavior of the stresses near the tip of interface cracks, this definition cannot be applied to the cracks lying on the bimaterial interface. A proper definition for the bimaterial stress intensity factors has been given by Hwu (1993) as

$$\begin{Bmatrix} K_{II} \\ K_I \\ K_{III} \end{Bmatrix} = \lim_{\substack{r\to 0 \\ \theta=0}} \sqrt{2\pi r}\boldsymbol{\Lambda}\langle (r/\ell)^{-i\varepsilon_*}\rangle \boldsymbol{\Lambda}^{-1} \begin{Bmatrix} \sigma_{r\theta} \\ \sigma_{\theta\theta} \\ \sigma_{\theta z} \end{Bmatrix}, \tag{3.2a}$$

or in matrix form

$$\mathbf{k} = \lim_{\substack{r\to 0 \\ \theta=0}} \sqrt{2\pi r}\boldsymbol{\Lambda}\langle (r/\ell)^{-i\varepsilon_*}\rangle \boldsymbol{\Lambda}^{-1}\boldsymbol{\phi}_{,r}, \tag{3.2b}$$

where

$$\boldsymbol{\Lambda} = [\,\tilde{\mathbf{q}}_1 \quad \tilde{\mathbf{q}}_2 \quad \tilde{\mathbf{q}}_3\,]. \tag{3.3a}$$

ε_*, $\tilde{\mathbf{q}}_*$, $* = 1, 2, 3$, are the eigenvalues and eigenvectors of

$$(\mathbf{M}^* - e^{2\pi\varepsilon}\overline{\mathbf{M}}^*)\tilde{\mathbf{q}} = \mathbf{0}, \tag{3.3b}$$

in which $\mathbf{M}^*$ is the bimaterial matrix related to the material eigenvector matrices $\mathbf{A}_i$, $\mathbf{B}_i$, $i = 1, 2$ (Hwu, 1993; Ting, 1996). In (3.2), ℓ is a length parameter which may be chosen arbitrarily as long as it is held fixed when specimens of a given material pair are compared. Different values of ℓ will not alter the magnitude of $\mathbf{k}$ but will change its phase angle. In application, the reference length ℓ is usually selected to be the crack length.

Combining (3.1) and (3.2), and considering the consistence of definitions, we now propose a unified definition for the stress intensity factors of interface corners, which is also applicable for the cracks in homogeneous materials or bimaterial interfaces, as

$$\begin{Bmatrix} K_{II} \\ K_I \\ K_{III} \end{Bmatrix} = \lim_{\substack{r\to 0 \\ \theta=0}} \sqrt{2\pi} r^{1-\lambda_R}\boldsymbol{\Lambda}\langle (r/\ell)^{-i\varepsilon_*}\rangle \boldsymbol{\Lambda}^{-1} \begin{Bmatrix} \sigma_{r\theta} \\ \sigma_{\theta\theta} \\ \sigma_{\theta z} \end{Bmatrix}, \tag{3.4a}$$

or in matrix form

$$\mathbf{k} = \lim_{\substack{r\to 0 \\ \theta=0}} \sqrt{2\pi} r^{1-\lambda_R}\boldsymbol{\Lambda}\langle (r/\ell)^{-i\varepsilon_*}\rangle \boldsymbol{\Lambda}^{-1}\boldsymbol{\phi}_{,r}, \tag{3.4b}$$

in which $\boldsymbol{\Lambda}$ is a matrix related to the wedge configurations and properties. In general, if λ_c is real, i.e., $\varepsilon_* = 0$, $\boldsymbol{\Lambda}$ is not required for the definition of $\mathbf{k}$ since $\boldsymbol{\Lambda}\langle (r/\ell)^{-i\varepsilon_*}\rangle \boldsymbol{\Lambda}^{-1}$ in (3.4) is equal to the identity matrix $\mathbf{I}$. With this understanding, only cases 4 and 5 shown in (2.10d and e) need a proper definition for the matrix $\boldsymbol{\Lambda}$.

Differentiating the stress function vector $\boldsymbol{\phi}(r,0)$ with respect to r for each case shown in (2.10a–e), and substituting the results into (3.4b), we can get the relations between the coefficients c_i (or simply c) and the stress intensity factors $\mathbf{k}$ as follows.

Case 1:

$$\mathbf{k} = \sqrt{2\pi} c \lambda_{\mathrm{R}} \mathbf{q}(0). \tag{3.5a}$$

Case 2:

$$\mathbf{k} = \sqrt{2\pi}\lambda_{\mathrm{R}} \boldsymbol{\Lambda}^{*}\mathbf{c}, \text{ where } \boldsymbol{\Lambda}^{*} = [\,\mathbf{q}_1(0) \quad \mathbf{q}_2(0)\,], \ \mathbf{c} = \begin{Bmatrix} c_1 \\ c_2 \end{Bmatrix}. \tag{3.5b}$$

Case 3:

$$\mathbf{k} = \sqrt{2\pi}\lambda_{\mathrm{R}} \boldsymbol{\Lambda}^{*}\mathbf{c}, \text{ where } \boldsymbol{\Lambda}^{*} = [\,\mathbf{q}_1(0) \quad \mathbf{q}_2(0) \quad \mathbf{q}_3(0)\,], \ \mathbf{c} = \begin{Bmatrix} c_1 \\ c_2 \\ c_3 \end{Bmatrix}. \tag{3.5c}$$

Case 4:

$$\mathbf{k}^{*} = \sqrt{2\pi}\boldsymbol{\Lambda}\langle(\lambda_{\mathrm{R}} + \mathrm{i}\varepsilon_{*})\ell^{\mathrm{i}\varepsilon_{*}}\rangle\mathbf{c}, \text{ where } \boldsymbol{\Lambda} = \left[\,\mathbf{q}^{*}(0) \quad \overline{\mathbf{q}^{*}(0)}\,\right], \ \mathbf{c} = \begin{Bmatrix} c \\ \bar{c} \end{Bmatrix}. \tag{3.5d}$$

Case 5:

$$\mathbf{k} = \sqrt{2\pi}\boldsymbol{\Lambda}\langle(\lambda_{\mathrm{R}} + \mathrm{i}\varepsilon_{*})\ell^{\mathrm{i}\varepsilon_{*}}\rangle\mathbf{c}, \text{ where } \boldsymbol{\Lambda} = \left[\,\mathbf{q}(0) \quad \overline{\mathbf{q}(0)} \quad \mathbf{q}_3(0)\,\right], \ \mathbf{c} = \begin{Bmatrix} c \\ \bar{c} \\ c_3 \end{Bmatrix}. \tag{3.5e}$$

Note that in case 2 $\boldsymbol{\Lambda}^{*}$ is a 3×2 matrix, while in case 3 $\boldsymbol{\Lambda}^{*}$ is a 3×3 matrix. In case 4 $\mathbf{k}^{*}$ is a 2×1 vector that could be $(K_{II}, K_I)^{\mathrm{T}}$ or $(K_I, K_{III})^{\mathrm{T}}$ depending on the contents of the 2×1 vector $\mathbf{q}^{*}(0)$ which may contain the first two components or the last two components of the 3×1 vector $\mathbf{q}(0)$. The associated diagonal matrix denoted by $\langle\rangle$ shown in (3.5d) is a 2×2 matrix in which each component is varied according to the subscript $* = 1, 2$, and $\varepsilon_1 = \varepsilon$, $\varepsilon_2 = -\varepsilon$. While in case 5, the associated diagonal matrix is a 3×3 matrix in which each component is varied according to the subscript $* = 1, 2, 3$ and $\varepsilon_1 = \varepsilon$, $\varepsilon_2 = -\varepsilon$, $\varepsilon_3 = 0$. Thus, $\boldsymbol{\Lambda}$ is a 2×2 matrix in case 4 and a 3×3 matrix in case 5.

A general matrix form for the relations shown in (3.5a–e) may be written as

$$\mathbf{k} = \sqrt{2\pi}\boldsymbol{\Lambda}\langle(\lambda_{\mathrm{R}} + \mathrm{i}\varepsilon_{*})\ell^{\mathrm{i}\varepsilon_{*}}\rangle\mathbf{c}, \tag{3.6}$$

in which the contents of matrices $\mathbf{k}$, $\boldsymbol{\Lambda}$ and $\mathbf{c}$ depend on whether the singular order is distinct or repeated, real or complex as those described in (2.10).

From the above discussion, we see that the definition for the stress intensity factors proposed in (3.4) is applicable not only to the interface corners but also to the cracks in homogeneous media or bimaterial interfaces. The conventional definition (3.1) is just a special case of (3.4) with $\lambda_{\mathrm{R}} = 1/2$ and $\varepsilon = 0$, while the definition for the bimaterial stress intensity factor (3.2) is a special case of (3.4) with $\lambda_{\mathrm{R}} = 1/2$. With this unified definition, it becomes possible that the failure criteria developed for the crack problems may be useful for the prediction of the failure of interface corners. Moreover, the fracture toughness measured from the standard crack specimen may also have a direct connection with the toughness of interface corners.

It should be noted that the unified definition proposed in (3.4) is valid only for the most critical singular order $\lambda_{\mathrm{c}} - 1$. For the cases that two or more but different eigenvalues exist in the range $0 < \mathrm{Re}(\lambda) < 1$, definition (3.4) cannot provide meaningful constant factors for the lower critical singular orders. For example, if $\boldsymbol{\phi}_{,r} \to c_1\lambda_{\mathrm{c}} r^{\lambda_{\mathrm{c}}-1}\mathbf{q}_1(\theta) + c_2\lambda_2 r^{\lambda_2-1}\mathbf{q}_2(\theta)$ when $r \to 0$, no constant values of $\mathbf{k}_2$ related to λ_2 can be got through the unified definition shown in (3.4). The possible way to get $\mathbf{k}_2$ is further modifying the definition with $\boldsymbol{\phi}_{,r}$

replaced by $\boldsymbol{\phi}^*_{,r}$ where $\boldsymbol{\phi}^*_{,r} = \boldsymbol{\phi}_{,r} - c_1\lambda_c r^{\lambda_c - 1}\mathbf{q}_1(\theta)$, which means that the near tip stresses of (3.4a) should be subtracted by the dominant portion of $\lambda_c - 1$. Since this will make the unified definition more complicated than before, in this paper we just focus on the stress intensity factors of the most critical singular order.

4. Path-independent *H*-integral for computing stress intensity factors

According to the definition of the stress intensity factors proposed in (3.4), to calculate their values we need to know the stresses near the tip of interface corners. However, due to the singular and possibly oscillatory behaviors of the near tip solutions (2.1) for multibonded anisotropic wedges, it is not easy to get convergent values for the stress intensity factors directly from the definition (3.4). To overcome this problem, several path-independent integrals have been proposed for the special cases of interface corners such as *J*-integral (Rice, 1968), *L*-Integral (Choi and Earmme, 1992), *M*-integral (Im and Kim, 2000) and *H*-integral (Sinclair et al., 1984) for crack problems. Since these integrals have a special feature that they are independent of paths, the complexity of stresses around the crack tip can then be avoided. The interface corners are usually in the status of mixed-mode intensity. Thus, employing *H*-integral to compute the stress intensity factors defined in (3.4) may be a good choice.

The path-independent *H*-integral is based on the reciprocal theorem of Betti and Rayleigh (Sokolnikoff, 1956). It states that: if an elastic body is subjected to two systems of body and surface forces, then the work that would be done by the first system in acting through the displacements due to the second system of forces is equal to the work that would be done by the second system in acting through the displacements due to the first system of forces. If we choose the first system to be the (actual) one we consider, and the second system to be the complementary (or called virtual) one. In the absence of body forces, this theorem can be written in the following form

$$\oint_C (\mathbf{u}^{\mathrm{T}}\hat{\mathbf{t}} - \hat{\mathbf{u}}^{\mathrm{T}}\mathbf{t})\,\mathrm{d}s = 0, \tag{4.1}$$

where $\mathbf{u}$ and $\mathbf{t}$ are the displacement and traction vectors of the actual system, and $\hat{\mathbf{u}}$ and $\hat{\mathbf{t}}$ are those of the complementary system. C is any closed contour in a simply connected region, which is selected to be $C_\varepsilon + C_1 + C_{R'} + C_2$ as shown in Fig. 1(b). Because the two outer surfaces of the multibonded wedges are considered to be free of tractions, $\mathbf{t} = \hat{\mathbf{t}} = \mathbf{0}$ along C_1 and C_2, and hence,

$$\int_{C_\varepsilon} (\mathbf{u}^{\mathrm{T}}\hat{\mathbf{t}} - \hat{\mathbf{u}}^{\mathrm{T}}\mathbf{t})\,\mathrm{d}s = -\int_{C_{R'}} (\mathbf{u}^{\mathrm{T}}\hat{\mathbf{t}} - \hat{\mathbf{u}}^{\mathrm{T}}\mathbf{t})\,\mathrm{d}s = \int_{C_R} (\mathbf{u}^{\mathrm{T}}\hat{\mathbf{t}} - \hat{\mathbf{u}}^{\mathrm{T}}\mathbf{t})\,\mathrm{d}s, \tag{4.2}$$

where both C_ε and C_R are the paths emanate from the lower wedge flank ($\theta = \theta_0$) to the upper wedge flank ($\theta = \theta_n$) counterclockwisely. In other words, the *H*-integral defined by

$$H = \int_\Gamma (\mathbf{u}^{\mathrm{T}}\hat{\mathbf{t}} - \hat{\mathbf{u}}^{\mathrm{T}}\mathbf{t})\,\mathrm{d}s, \tag{4.3}$$

is path-independent for free-free multibonded wedges when the path Γ emanates from θ_0 and terminates on θ_n in counterclockwise direction.

By shrinking the inner path C_ε inside the region dominated by the singular field and making a judicious choice for the complementary solution, we can get an analytical expression for the *H*-integral in terms of the coefficients c_i (or simply c) which have a direct relation with the stress intensity factors as shown in (3.5). Thus, if one can evaluate the *H*-integral from the other path far from the tip, through the path-independent property shown in (4.2) we can calculate the stress intensity factors. With this understanding, we will now try to find the suitable complementary solutions and then derive formulae for the coefficients c_i of each case shown in (2.10a–e).

Since the integral path can be selected arbitrarily from the lower wedge flank θ_0 to upper wedge flank θ_n, for simplicity we choose a circular counterclockwise path through the region dominated by the singular field. Along this path, the traction $\mathbf{t} = \boldsymbol{\phi}_{,\theta}/r$, which has been shown in (2.3b), and $\mathrm{d}s = r\,\mathrm{d}\theta$, so Eq. (4.3) becomes

$$H = \int_{\theta_0}^{\theta_n} (\mathbf{u}^{\mathrm{T}} \hat{\boldsymbol{\phi}}_{,\theta} - \hat{\mathbf{u}}^{\mathrm{T}} \boldsymbol{\phi}_{,\theta})\, \mathrm{d}\theta. \tag{4.4}$$

Case 1: Substituting the near tip solution (2.10a) into (4.4), we see that the suitable complementary solution, which will make the H-integral be independent of r, should be the one with eigenvalue $-\lambda_{\mathrm{R}}$, i.e.,

$$\hat{\mathbf{u}}(r,\theta) = \hat{c} r^{-\lambda_{\mathrm{R}}} \hat{\mathbf{p}}(\theta), \;\; \hat{\boldsymbol{\phi}}(r,\theta) = \hat{c} r^{-\lambda_{\mathrm{R}}} \hat{\mathbf{q}}(\theta), \tag{4.5}$$

where $\hat{\mathbf{p}}(\theta)$ and $\hat{\mathbf{q}}(\theta)$ can be obtained from (2.9a) with $\mathbf{u}_0$ determined by (2.8a) whose eigenvalue is $-\lambda_{\mathrm{R}}$. Thus, it is important to know whether $-\lambda$ is also an eigenvalue of $\mathbf{K}^{(3)}\mathbf{u}_0 = \mathbf{0}$ when λ is. Since the explicit expression of the determinant of matrix $\mathbf{K}^{(3)}$ is quite complicated, it is not easy to perform rigorous proof. Instead, numerical check has been done in this paper, which shows that when λ is a root of $\mathbf{K}^{(3)}\mathbf{u}_0 = \mathbf{0}$, so is $-\lambda$.

Substituting (2.10a) and (4.5) into (4.4) with $\hat{c} = 1$, we get

$$c = H^{*-1} H, \tag{4.6a}$$

where

$$H^* = \int_{\theta_0}^{\theta_n} \left\{ \mathbf{p}^{\mathrm{T}}(\theta) \hat{\mathbf{q}}'(\theta) - \hat{\mathbf{p}}^{\mathrm{T}}(\theta) \mathbf{q}'(\theta) \right\} \mathrm{d}\theta. \tag{4.6b}$$

The prime $\bullet'$ in (4.6b) denotes differentiation with respect to θ. Note that formula (4.6) is derived from the path through the singular field. By the path-independent property of H-integral, the value H appeared in (4.6a) can now be evaluated using (4.3) through any convenient path Γ far away from the tip. In (4.3), the displacement $\mathbf{u}$ and traction $\mathbf{t}$ of the actual state can be obtained from any other methods such as finite element or boundary element method, while $\hat{\mathbf{u}}$ and $\hat{\mathbf{t}}$ of the virtual state is from the complementary solution (4.5) whose $\hat{c} = 1$ and $\hat{\mathbf{t}} = \partial \hat{\boldsymbol{\phi}} / \partial s$.

Case 2: Similar to the discussion of Case 1, the suitable complementary solution will be the one associated with eigenvalue $-\lambda_{\mathrm{R}}$, i.e.,

$$\begin{aligned} \hat{\mathbf{u}}(r,\theta) &= r^{-\lambda_{\mathrm{R}}} \{ \hat{c}_1 \hat{\mathbf{p}}_1(\theta) + \hat{c}_2 \hat{\mathbf{p}}_2(\theta) \}, \\ \hat{\boldsymbol{\phi}}(r,\theta) &= r^{-\lambda_{\mathrm{R}}} \{ \hat{c}_1 \hat{\mathbf{q}}_1(\theta) + \hat{c}_2 \hat{\mathbf{q}}_2(\theta) \}. \end{aligned} \tag{4.7}$$

Substituting (2.10b) and (4.7) into (4.4) with $\hat{c}_1 = 1$, $\hat{c}_2 = 0$, and $\hat{c}_1 = 0$, $\hat{c}_2 = 1$, respectively, we get

$$\begin{aligned} H_1 &= c_1 H_{11}^* + c_2 H_{12}^*, \\ H_2 &= c_1 H_{21}^* + c_2 H_{22}^*, \end{aligned} \tag{4.8a}$$

where

$$H_{ij}^* = \int_{\theta_0}^{\theta_n} \left\{ \mathbf{p}_j^{\mathrm{T}}(\theta) \hat{\mathbf{q}}_i'(\theta) - \hat{\mathbf{p}}_i^{\mathrm{T}}(\theta) \mathbf{q}_j'(\theta) \right\} \mathrm{d}\theta, \;\; i,j = 1,2, \tag{4.8b}$$

and H_1 is the value calculated from (4.3) with $\hat{c}_1 = 1$, $\hat{c}_2 = 0$ for the complementary solution, while H_2 is the one associated with $\hat{c}_1 = 0$, $\hat{c}_2 = 1$. From (4.8), the coefficient c_i can now be evaluated by simply matrix inversion as

$$\begin{Bmatrix} c_1 \\ c_2 \end{Bmatrix} = \begin{bmatrix} H_{11}^* & H_{12}^* \\ H_{21}^* & H_{22}^* \end{bmatrix}^{-1} \begin{Bmatrix} H_1 \\ H_2 \end{Bmatrix}. \tag{4.9}$$

Case 3: Similar to Case 2, the complementary solution can be written as

$$\begin{aligned} \hat{\mathbf{u}}(r,\theta) &= r^{-\lambda_{\mathrm{R}}} \{ \hat{c}_1 \hat{\mathbf{p}}_1(\theta) + \hat{c}_2 \hat{\mathbf{p}}_2(\theta) + \hat{c}_3 \hat{\mathbf{p}}_3(\theta) \}, \\ \hat{\boldsymbol{\phi}}(r,\theta) &= r^{-\lambda_{\mathrm{R}}} \{ \hat{c}_1 \hat{\mathbf{q}}_1(\theta) + \hat{c}_2 \hat{\mathbf{q}}_2(\theta) + \hat{c}_3 \hat{\mathbf{q}}_3(\theta) \}. \end{aligned} \tag{4.10}$$

Substituting (2.10c) and (4.10) into (4.4) with $\hat{c}_1 = 1$, $\hat{c}_2 = 0$, $\hat{c}_3 = 0$, and $\hat{c}_1 = 0$, $\hat{c}_2 = 1$, $\hat{c}_3 = 0$, and $\hat{c}_1 = 0$, $\hat{c}_2 = 0$, $\hat{c}_3 = 1$, respectively, and then by matrix inversion, we get

$$\begin{Bmatrix} c_1 \\ c_2 \\ c_3 \end{Bmatrix} = \begin{bmatrix} H_{11}^* & H_{12}^* & H_{13}^* \\ H_{21}^* & H_{22}^* & H_{23}^* \\ H_{31}^* & H_{32}^* & H_{33}^* \end{bmatrix}^{-1} \begin{Bmatrix} H_1 \\ H_2 \\ H_3 \end{Bmatrix}, \tag{4.11}$$

in which H_{ij}^* has the same definition as (4.8b) for $i, j = 1, 2, 3$; H_1 is the value calculated from (4.3) with $\hat{c}_1 = 1$, $\hat{c}_2 = 0$, $\hat{c}_3 = 0$ for the complementary solution, H_2 is the one associated with $\hat{c}_1 = 0$, $\hat{c}_2 = 1$, $\hat{c}_3 = 0$, while H_3 is the one associated with $\hat{c}_1 = 0$, $\hat{c}_2 = 0$, $\hat{c}_3 = 1$.

Case 4: Each term of the solution shown in (2.10d), although its value is complex, satisfies all the basic equations and boundary conditions for the multibonded wedges. In this sense, the coefficient c, even is complex, can also be evaluated by the way of Case1. That is, with the complementary solution

$$\hat{\mathbf{u}}(r,\theta) = \hat{c} r^{-(\lambda_R + i\varepsilon)} \hat{\mathbf{p}}(\theta), \ \hat{\boldsymbol{\phi}}(r,\theta) = \hat{c} r^{-(\lambda_R + i\varepsilon)} \hat{\mathbf{q}}(\theta), \tag{4.12}$$

c is related to the H-integral by (4.6a), i.e., $c = H^{*-1}H$, where H^* and H are, respectively, calculated from (4.6b) and (4.3) with $\hat{c} = 1$. Similarly, the coefficient $\bar{c}$ can also be calculated by (4.6a) with a complementary solution having exponent $-(\lambda_R - i\varepsilon)$ of r. Since c and $\bar{c}$ are complex conjugate, their results calculated separately by (4.6) can be used as a check for correctness.

Case 5: As the explanation described for case 4, in this case λ_R and $\lambda_R \pm i\varepsilon$ can be treated as three distinct roots. The complementary solutions associated with eigenvalues λ_R and $\lambda_R + i\varepsilon$ have been shown, respectively, in (4.5) and (4.12). Their associated coefficients c_3 and c can therefore be evaluated separately by (4.6). The coefficient $\bar{c}$ associated with eigenvalue $\lambda_R - i\varepsilon$ is then obtained by taking the conjugate of c.

From the above discussion, we see that the coefficients c_i (or simply c) can be evaluated from the relations (4.6), (4.9), (4.11) or (4.12) through the path-independent H-integral. A general matrix form for these relations can then be shown as

$$\mathbf{c} = \mathbf{H}^{*-1}\mathbf{h}, \tag{4.13}$$

where the dimensions of vector $\mathbf{c}$, matrix $\mathbf{H}^*$ and vector $\mathbf{h}$ depend on whether the singular order is distinct or repeated, real or complex as those described in (2.10). The component H_{ij}^* of $\mathbf{H}^*$ is calculated through (4.8b), whereas the component H_i of $\mathbf{h}$ is calculated from the H-integral defined in (4.3) through any convenient path Γ emanating from θ_0 and terminating on θ_n in counterclockwise direction. When calculating H_i through (4.3), $\mathbf{u}$ and $\mathbf{t}$ of the actual state can be obtained from any other methods, while $\hat{\mathbf{u}}$ and $\hat{\mathbf{t}}$ of the virtual state is from the complementary solution such as (4.5), (4.7), (4.10) with $\hat{c}_i = 1$ and $\hat{c}_j = 0$, $j \neq i$. Combining (3.6) and (4.13), the relation between the stress intensity factors $\mathbf{k}$ and the H-integral $\mathbf{h}$ is obtained as

$$\mathbf{k} = \sqrt{2\pi}\boldsymbol{\Lambda}\langle(\lambda_R + i\varepsilon_*)\ell^{i\varepsilon_*}\rangle\mathbf{H}^{*-1}\mathbf{h}. \tag{4.14}$$

With this relation, the stress intensity factors defined in (3.4) can be computed in a stable and efficient way no matter what kind of interface corners is considered.

5. Numerical examples

A unified definition for the stress intensity factors of cracks, interface cracks and interface corners is proposed in Eq. (3.4). No matter what kind of stress singularity occurs for the general interface corners/cracks, (distinct or repeated, real or complex), an efficient and stable approach of calculating the stress intensity factors is suggested by using the relation (4.14) with the path-independent H-integral defined in (4.3). Detailed studies about the convergency and efficiency of the H-integral as well as the validity of the range and shape of the path have been done through several different kinds of examples. To save the space of this paper, only selected examples are shown to illustrate the versatility of the unified definition, such as (1) cracks in homogeneous isotropic or anisotropic materials, (2) central or edge notch in isotropic materials, (3) interface cracks between two dissimilar isotropic materials, and (4) interface corners between two dissimilar materials. In the first example, the singular order is $-1/2$ which is a repeated root associated with opening, shearing and tearing stress intensity factors. Example 2 is a case of single wedge problem whose singular order is generally less than that of crack (here, we compare the absolute value of the singular order), and is generally real. Example 3

shows the variation of the stress intensity factors of the interface cracks versus the stiffness ratio of the two materials. No matter what kinds of combination of the bimaterials, the singular orders of this example are always $-1/2$ and $-1/2 \pm i\varepsilon$, which belong to the category of case 5 discussed in Section 2. The last example shows a typical example of interface corners, which occurs frequently in electric devices. The singular order of this case is generally complex.

Note that in the following calculation, the stresses and displacements of the actual system are obtained from the commercial finite element software ANSYS. For convenience, the paths are usually selected to pass through Gauss points or nodal points. Otherwise, interpolation technique is used to get the values of displacements and stresses. In our example all the integration paths are selected to pass through nodal points. Since the numerical output will depend on element meshes and integral paths, both studies have been done in (Kuo, 2006) before performing the following examples. Kuo's results show that the convergent and stable values will be obtained if the normalized element size b/a is less than 0.05 and the normalized integral paths r/a lie within $0.2 < r/a < 0.8$, where b is the grid size of the meshes in the region $2a \times 2a$ centered on the crack/notch tips, r is the radius of circular integral path and a is the crack or notch length.

It should be noted that although the path independency of H-integral has been proved theoretically in Section 4, numerical studies through several different shapes and ranges of paths show that the stress intensity factors calculated from the paths with r/a less than 0.2 become unstable and will change rapidly, which may come from the incorrect stress information near the crack/notch tip provided by FEA. Therefore, when using H-integral to calculate the stress intensity factors we avoid to take the values near the range of $r/a < 0.2$, which is the advantage of the path-independent integrals.

Example 1. Cracks in homogeneous isotropic or anisotropic materials

Since this kind of problems has been done vastly in the literature, for the purpose of comparison we now select two cases presented by Stern et al. (1976). One is an edge crack in a rectangular homogeneous isotropic plate subjected to uniform tension, and the other is the same plate subjected to uniform end shear and fully clamped at the other end, as shown in Fig. 2a and b, respectively. The Young's modulus E and Poisson's ratio v of the plate are: $E = 300$ GPa, $v = 0.25$. The uniform stress applied at the end of the plate is $\sigma = 1$ MPa. Table 1 is the comparison of our results with those presented by Stern et al. (1976), which shows that our results well agree with those of Stern et al. (1976). Moreover, the path-independent property of H-integral is confirmed through this numerical computation in which four different paths used in our calculation are shown in Fig. 3. Following the requirement that the normalized element size b/a be less than 0.05, the results shown in Table 1 are based on the FEA meshes of 8284 elements and 25,331 nodes.

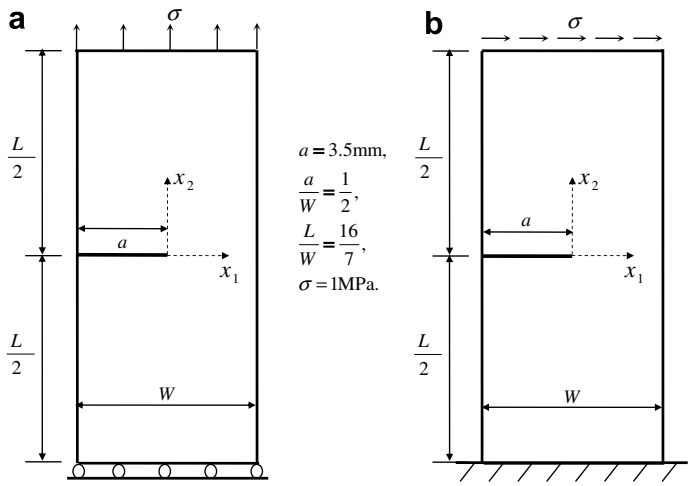

Fig. 2. Schematic diagram of an edge crack in an homogeneous isotropic plate subjected to (a) uniform tension; (b) uniform end shear.

Table 1
Stress intensity factors of edge cracks in isotropic media

Present		
(i) Uniform tension		
$r = 0.225$		$K_I = 9.254$
$r = 0.375$		$K_I = 9.309$
$r = 0.450$		$K_I = 9.359$
$r = 0.600$		$K_I = 9.367$
Stern et al. (1976)		$K_I = 9.300$
(ii) Uniform end shear		
$r = 0.225$	$K_I = 33.448$	$K_{II} = 4.446$
$r = 0.375$	$K_I = 33.675$	$K_{II} = 4.406$
$r = 0.450$	$K_I = 33.745$	$K_{II} = 4.459$
$r = 0.600$	$K_I = 33.725$	$K_{II} = 4.483$
Stern et al. (1976)	$K_I = 34.000$	$K_{II} = 4.550$

Unit: r – mm; K_I and K_{II} – MPa $*$ mm$^{0.5}$.

To show that the proposed approach is not only valid for isotropic materials but also for the most general anisotropic materials, a central crack embedded in an anisotropic plate is considered (Fig. 4). The plate is subjected to uniform stress $\sigma = 10$ MPa at far ends. The anisotropic materials are made by rotating the principal direction of an orthotropic material 45 degrees (i.e. $\gamma = 45°$ in Fig. 4). The material properties of the orthotropic material are

$$E_{11} = 134.45\ \text{GPa}, \quad E_{22} = E_{33} = 11.03\ \text{GPa},$$
$$G_{12} = G_{13} = 5.84\ \text{GPa}, \quad G_{23} = 2.98\ \text{GPa},$$
$$\nu_{12} = \nu_{13} = 0.301, \quad \nu_{23} = 0.49.$$

To compare our results with the analytical solution for a crack in the infinite anisotropic media, $a = 1$ mm, $a/W = 1/60$ and $a/L = 1/58$ are used in our example to approximate an infinite plate. Table 2 shows that the values of K_I calculated from H-integral well agree with the analytical solution $K_I = \sigma\sqrt{\pi a}$.

Example 2. Central or edge notch in isotropic materials

Notch problems such as the one shown in Fig. 5 have also been studied vastly in the literature. However, in the literature most of the stress intensity factors of the notches are defined in the following way:

$$\sigma_{\theta\theta}(\theta = 0) = K_I r^{\lambda-1}, \quad \sigma_{r\theta}(\theta = 0) = K_{II} r^{\lambda-1}, \quad \sigma_{\theta z}(\theta = 0) = K_{III} r^{\lambda-1}$$

Although they are correct in the sense of stress intensity, they are different from the conventional definition of cracks by a scaling factor $\sqrt{2\pi}$. Moreover, it will cause trouble when λ is a repeated or complex root, like those discussed in Section 2 for Cases 2–5. Since crack is a special case of notches whose notch angle $\alpha = 0°$ (Fig. 5), it is better that the stress intensity factors are defined by the same definition. Thus, in this example the comparison is done by the using the definition proposed in Eq. (3.4). Table 3 shows the stress intensity factors of central notch and edge notch for $\alpha = 90°$, whose singular order $\lambda_c - 1 = -0.456$. Again, good agreement is shown in the comparison between our results and those of Dunn et al. (1997). The material constants and load considered in this example are: $E = 300$ GPa, $\nu = 0.25$, $a = 1$ mm, $a/W = 1/20$, and $a/L = 1/60$, and $\sigma = 10$ MPa.

Example 3. Interface cracks between two dissimilar isotropic materials

Consider a center crack or edge crack lying along the interface between two dissimilar isotropic materials. The geometry and loading of this problem are shown in Fig. 6. The reference length used in the definition (3.4) is selected to be half of the crack length for center crack and crack length for edge crack, which are all denoted by a in Fig. 6. Both of the materials above and below the interface are isotropic. Their properties are $E^{(1)} = 300$ GPa, $\nu^{(1)} = \nu^{(2)} = 0.25$, and $E^{(2)}$ varies according to the stiffness ratio $E^{(2)}/E^{(1)}$ given in Table 4. The singular order and the stress intensity factor versus the stiffness ratio for the

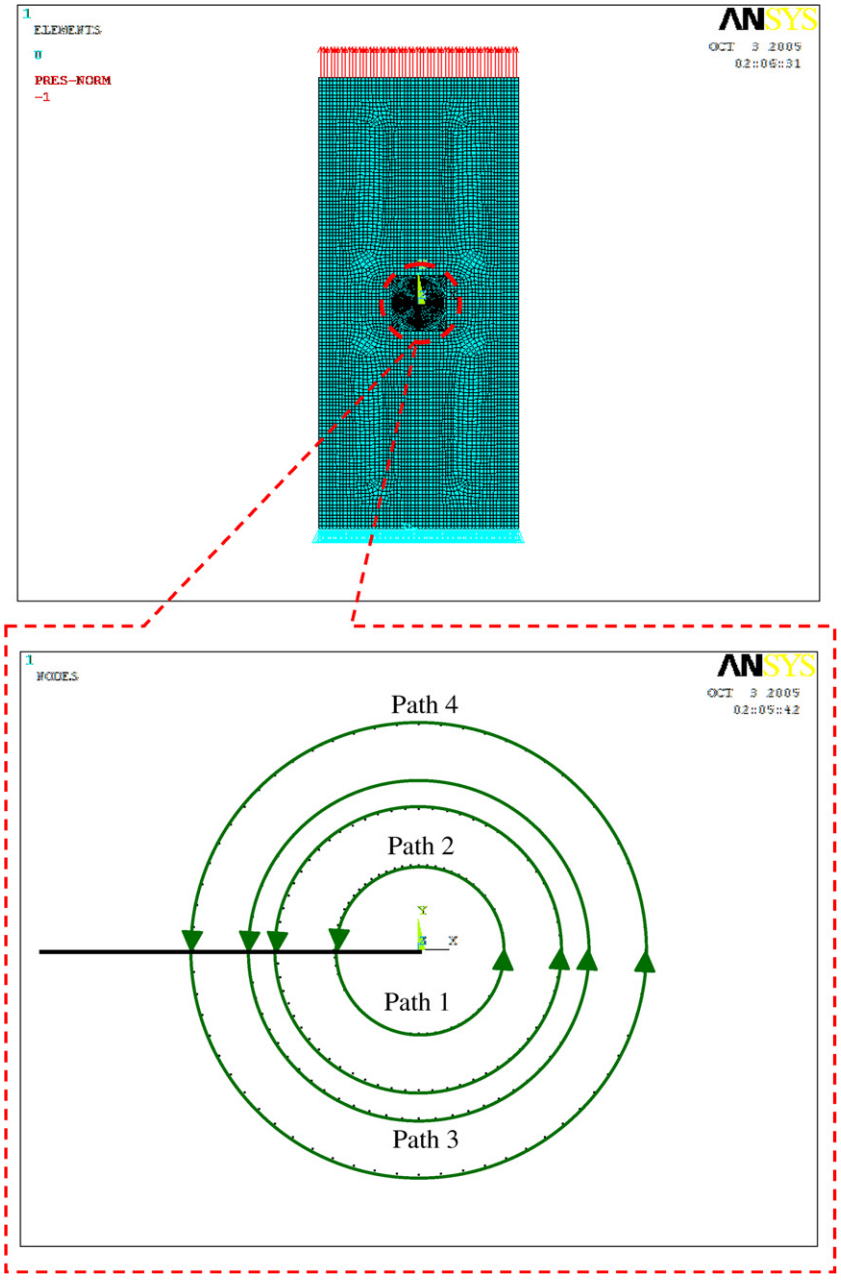

Fig. 3. *H*-integral paths for example 1.

center interface crack and edge interface crack are presented in Table 4. The reference values shown in Table 4 are those calculated from the analytical solutions for the center interface cracks in infinite plates (Rice, 1988; Hwu, 1993). Since the values of a/W and a/L have been purposely selected to be small enough to simulate the infinite plates, our results are well agreed with the reference values. Note that the selection of the reference length ℓ will not alter the magnitude of $\mathbf{k}$ (means $\sqrt{K_I^2 + K_{II}^2}$) but will change the individual values of K_I and K_{II}, and hence when comparing with other solutions one should be careful about its selection.

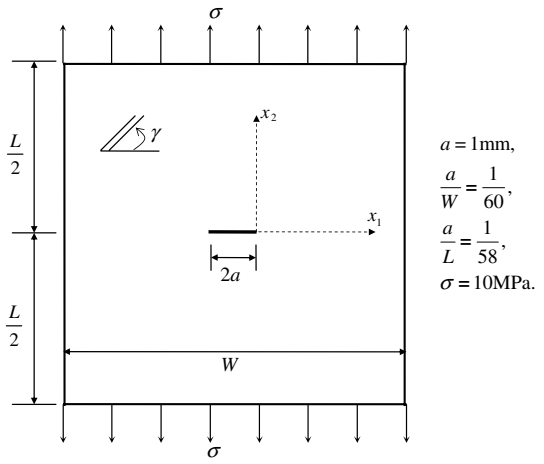

Fig. 4. Schematic diagram of a central crack in an anisotropic plate.

Table 2
Stress intensity factors of central cracks in anisotropic media

Present	
$r = 0.500$	$K_I = 17.633$
$r = 0.600$	$K_I = 17.631$
$r = 0.700$	$K_I = 17.630$
$r = 0.800$	$K_I = 17.636$
Analytic solution	
$\sigma\sqrt{\pi a}$	$K_I = 17.725$

Unit: r – mm; K_I – MPa $*$ mm$^{0.5}$.

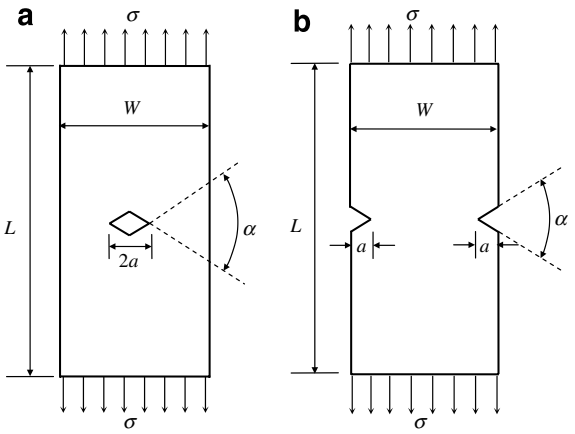

Fig. 5. Schematic diagrams of notches in isotropic plates: (a) central notch (b) edge notch.

Example 4. Interface corners between two dissimilar materials

In this example we consider an interface corner between two dissimilar materials subjected to uniform tension $\sigma = 10$ MPa at far ends. The geometry, loading, and boundary conditions are shown in Fig. 7. The interface length $d = 5$ mm, the reference length ℓ used in the definition (3.4) is selected to be 10 mm. The material above the interface is isotropic whose properties are: $E = 10$ GPa and $v = 0.2$, while the other portion is orthotropic whose properties are the same as those given in Example 1.

Table 3
Stress intensity factors of central notches and edge notches

K_I		
$\alpha = 90°$	Central notch	Edge notch
Present		
$r = 0.540$	22.490	23.152
$r = 0.630$	22.482	23.146
$r = 0.720$	22.479	23.143
Dunn et al. (1997)	22.464	23.191

Unit: r – mm; K_I – MPa $*$ mm$^{0.456}$.

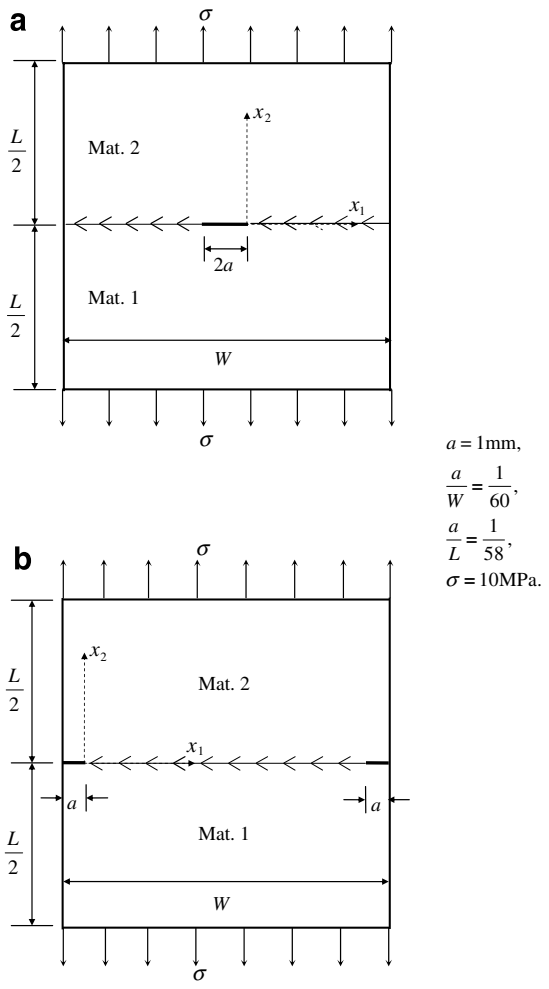

Fig. 6. Interface cracks between two dissimilar isotropic materials: (a) central crack (b) edge crack.

The singular order of this problem is calculated to be $\lambda_c = 0.467–0.037i$. The stress intensity factors $\mathbf{k}$ *versus* the near tip distance r are shown in Table 5, Figs. 8 and 9 for the values calculated from (3.4) and (4.14). Fig. 8 shows that the values of K_I and K_{II} calculated directly from the definition (3.4) become unstable when $r \to 0$, which causes trouble to determine the limiting values. While in Fig. 9, K_I and K_{II} calculated from H-integral are quite independent of the paths, in which r stands for the radius of the circular path. The range of r shown in Fig. 8 is $0.0006 < r < 0.017$ while that of Fig. 9 is $0.3 < r < 0.8$. The former is the near tip region, from which

Table 4
Stress intensity factors of interface cracks *vs.* ratio of Young's modulus $E^{(2)}/E^{(1)}$

$E^{(2)}/E^{(1)}$	$\lambda_c - 1$	K_I	K_I^*	K_{II}	K_{II}^*
Center interface crack					
0.01	−0.5000 + 0.1080i	16.4802	17.9611	2.2408	2.4914
0.1	−0.5000 + 0.0891i	17.0004	17.8856	1.9252	2.0579
0.2	−0.5000 + 0.0719i	17.2926	17.8296	1.5916	1.6636
0.3	−0.5000 + 0.0578i	17.4543	17.7923	1.2948	1.3365
0.4	−0.5000 + 0.0458i	17.5508	17.7671	1.0347	1.0599
0.5	−0.5000 + 0.0355i	17.6108	17.7502	0.8067	0.8223
0.6	−0.5000 + 0.0266i	17.6486	17.7389	0.6058	0.6157
0.7	−0.5000 + 0.0187i	17.6720	17.7317	0.4280	0.4342
0.8	−0.5000 + 0.0118i	17.6856	17.7274	0.2697	0.2732
0.9	−0.5000 + 0.0056i	17.6925	17.7252	0.1277	0.1293
1.0	−0.5000 + 0.0000i	17.6844	17.7245	0.0000	0.0000

$E^{(2)}/E^{(1)}$	$\lambda_c - 1$	K_I	K_{II}
Edge interface crack			
0.01	−0.5000 + 0.1080i	29.7183	8.3921
0.1	−0.5000 + 0.0891i	26.1536	6.1506
0.2	−0.5000 + 0.0719i	23.8200	4.5734
0.3	−0.5000 + 0.0578i	22.3822	3.4920
0.4	−0.5000 + 0.0458i	21.4531	2.6903
0.5	−0.5000 + 0.0355i	20.8368	2.0641
0.6	−0.5000 + 0.0266i	20.4263	1.5543
0.7	−0.5000 + 0.0187i	20.1538	1.1240
0.8	−0.5000 + 0.0118i	19.9800	0.7548
0.9	−0.5000 + 0.0056i	19.8760	0.4300
1.0	−0.5000 + 0.0000i	19.8375	0.0000

Unit: K_I, K_{II}, K_I^* and K_{II}^* – MPa * $mm^{0.5}$.
Note: K_I^* and K_{II}^* are the values for infinite plates calculated from the formulae provided in (Rice, 1988; Hwu, 1993).

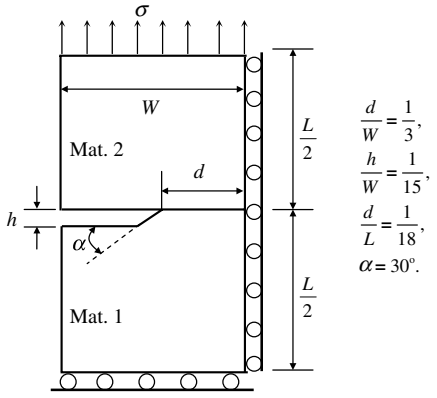

Fig. 7. Schematic diagram of interface corner between dissimilar materials.

the results are usually unstable, however, it is unavoidable because the definition requires $r \to 0$; whereas the latter is away from the unstable region, which is the advantage of the path-independent integrals. Since the calculation from definition (3.4) requires r approach to zero, the values obtained from the stable region like that used in Fig. 9 are not correct and are not near constant, which can be seen from the values shown in Table 5.

Example 5. Effects of interface corner angles

Table 5
Stress intensity factors of interface corners calculated by (3.4) and (4.14)

	K_I	K_{II}
H-integral, Eq. (4.14)		
$r = 0.3375$	72.5264	8.8041
$r = 0.4500$	72.6637	9.0112
$r = 0.5625$	72.7715	9.1537
$r = 0.6750$	72.8586	9.2604
$r = 0.7875$	72.9351	9.3466
Definition, Eq. (3.4)		
$r = 0.0006$	69.8714	19.3757
:	As shown in Fig. 8.	As shown in Fig. 8.
:		
$r = 0.0169$	72.9669	7.5119
$r = 0.0281$	71.6144	10.4688
$r = 0.0422$	71.6611	7.4874
$r = 0.1125$	72.5257	8.1184
$r = 0.2250$	73.3319	6.5985
$r = 0.3375$	74.4222	6.5252
$r = 0.4500$	75.0793	6.3836
$r = 0.5625$	75.6997	6.2747
$r = 0.6750$	76.3009	6.1677
$r = 0.7875$	76.8890	6.0497
$r = 0.9000$	77.5679	5.9326

Unit: r – mm; K_I and K_{II} – MPa $*\text{mm}^{0.467}$.

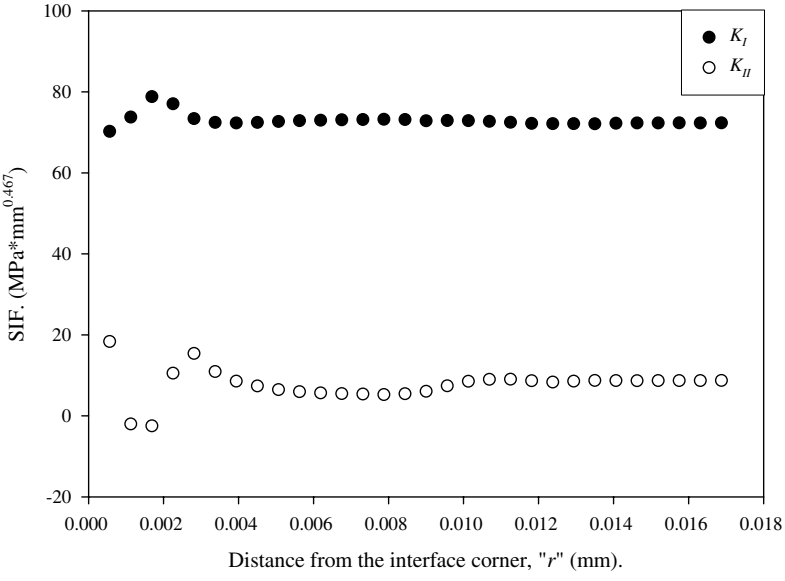

Fig. 8. Stress intensity factors of interface corners calculated directly from the definition, Eq. (3.4).

It is known that the interface crack is a special case of interface corner with angle $\alpha = 0$ (Fig. 7), and the crack in homogeneous materials is a special case of interface crack between two identical materials. Therefore, with the unified definition proposed in this paper, it is interesting to know the variation of stress intensity factors with respect to corner angles and material properties (Kuo, 2006). Followings are the results based upon Example 4 (see Fig. 7) by varying the angle α of interface corner. All the stress intensity factors in this example are calculated from (4.14) with circular integral path of $r = 0.7875$ mm.

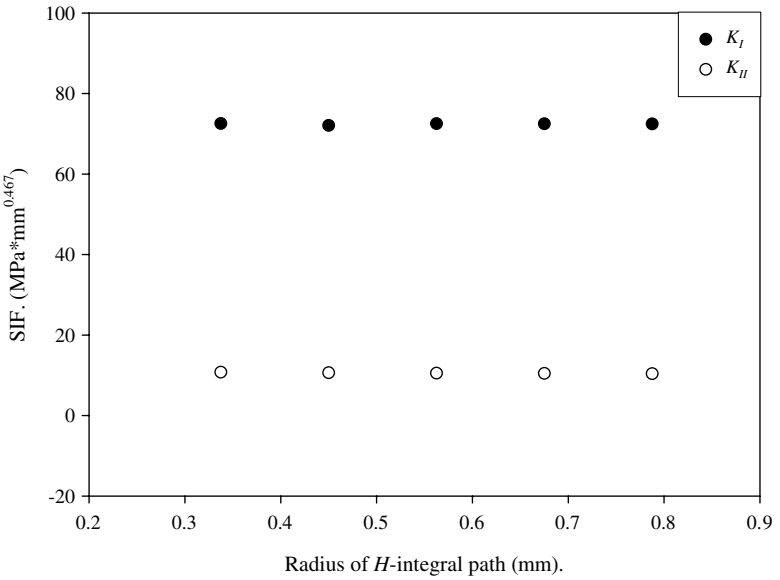

Fig. 9. Stress intensity factors of interface corners calculated indirectly from H-integral, Eq. (4.14).

Fig. 10a shows the first three orders of stress singularity for interface corner $\alpha = 0^\circ \sim 160^\circ$, while Fig. 10b shows their corresponding stress intensity factors of the most critical singular order $\lambda_c - 1$. It is interesting to see that $\lambda_c - 1$ change from real value to complex value when $\alpha < 40^\circ$ and their associated stress intensity factors also change abruptly at $\alpha = 40^\circ$. In this example, all the second and third orders of stress singularity, $\lambda_2 - 1$ and $\lambda_3 - 1$, are real values, and their associated stress intensity factors are not presented since the unified definition proposed in this paper is defined only for the most critical order of stress singularity. When $\alpha = 0$ the interface corner becomes the interface crack, and its associated orders of stress singularity reduce to the values $\lambda - 1 = -0.5,\ -0.5 \pm 0.0633\mathrm{i}$ (as shown in Fig. 10a), which are exactly the same as those calculated by the closed form solution (Ting, 1986).

6. Conclusions

The near tip solutions for the general interface corners have been divided into five categories depending on whether the singular order is distinct or repeated, real or complex. These five categories cover all the possibilities of the interface corners including the homogenous cracks and interface cracks. Based upon the conventional definitions for the cracks in homogeneous materials and the interface cracks in bimaterials, a unified definition for the stress intensity factors of general interface corners and cracks is proposed in (3.4). With the knowledge of the near tip solutions, an important relation connecting this newly defined stress intensity factor and the path-independent H-integral is obtained in (4.14). To calculate the stress intensity factors through this relation, both the near tip solutions associated with the critical singular order λ_c and the complementary solutions associated with $-\lambda_c$ are needed, which can be obtained from (2.8)–(2.10). With these solutions, the H-integral can be calculated effectively by inputting the displacements and tractions of the actual state directly from any numerical method such as finite element or boundary element method. To illustrate the versatility of the unified definition of the stress intensity factors and the accuracy and efficiency of the H-integral, five different kinds of examples are shown such as cracks/notches in homogeneous materials and interface cracks/corners between dissimilar materials.

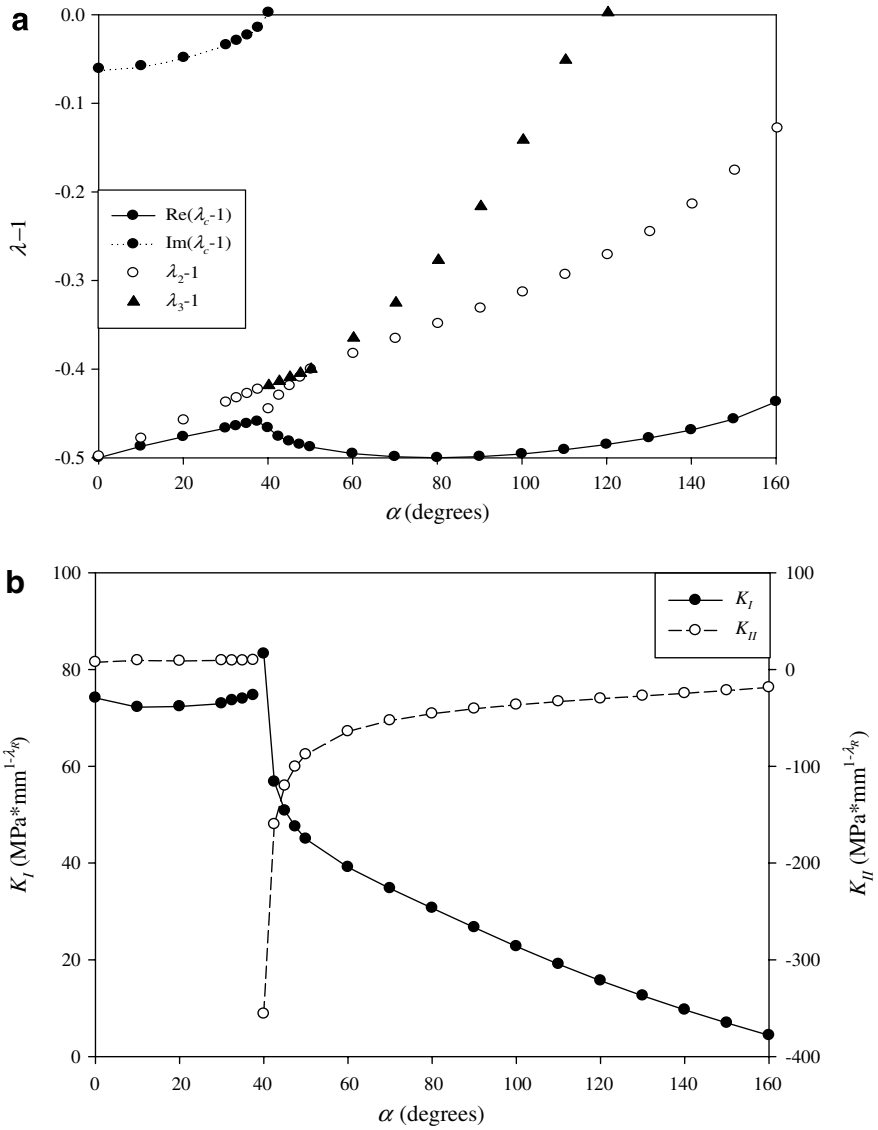

Fig. 10. (a) Orders of stress singularity $\lambda - 1$ *versus* angles of interface corner α. (b) Stress intensity factors *versus* angles of interface corner α.

Acknowledgments

The authors thank the National Science Council, Taiwan, R.O.C. for support through Grant NSC 90-2212-E-006-149 and NSC 94-2212-E-006-081.

References

Broek, D., 1974. Elementary Engineering Fracture Mechanics. Noordhoff International Publication, Leyden.

Choi, N.Y., Earmme, Y.Y., 1992. Evaluation of stress intensity factors in a circular arc-shaped interfacial crack using *L*-integral. Mechanics of Materials 14, 141–153.

Dunn, M.L., Suwito, W., Cunningham, S., 1997. Stress intensities at notch singularities. Engineering Fracture Mechanics 57 (4), 417–430.

Gao, H., Abbudi, M., Barnett, D.M., 1992. On interfacial crack-tip field in anisotropic elastic solids. Journal of the Mechanics and Physics of Solids 40, 393–416.

Hwu, C., 1993. Explicit solutions for collinear interface crack problems. International Journal of Solids and Structures 30 (3), 301–312.
Hwu, C., Omiya, M., Kishimoto, K., 2003. A key matrix N for the stress singularity of the anisotropic elastic composite wedges. JSME International Journal Series A 46 (1), 40–50.
Hwu, C., Lee, W.J., 2004. Thermal effect on the singular behavior of multi-bonded anisotropic wedges. Journal of Thermal Stresses 27 (2), 111–136.
Im, S., Kim, K.S., 2000. An application of two-state *M*-integral for computing the intensity of the singular near-tip field for a generic wedge. Journal of the Mechanics and Physics of Solids 48, 129–151.
Kuo, T.L., 2006. Stress Intensity Factors for Interface Corners., MS thesis, Institute of Aeronautics and Astronautics, National Cheng Kung University.
Labossiere, P.E.W., Dunn, M.L., 1999. Stress intensities at interface corners in anisotropic bimaterials. Engineering Fracture Mechanics 62, 555–575.
Rice, J.R., 1968. A path independent integral and the approximate analysis of strain concentration by notches and cracks. ASME Journal of Applied Mechanics 35, 379–386.
Rice, J.R., 1988. Elastic fracture mechanics concepts for interfacial Cracks. ASME Journal of Applied Mechanics 55, 98–103.
Sinclair, G.B., Okajima, M., Griffen, J.H., 1984. Path independent integrals for computing stress intensity factors at sharp notches in elastic plates. International Journal for Numerical Methods in Engineering 20, 999–1008.
Sokolnikoff, I.S., 1956. Mathematical Theory of Elasticity, second ed. McGraw Hill.
Stern, M., Becker, E.B., Dunham, R.S., 1976. A contour integral computation of mixed-bode stress intensity factors. International Journal of Fracture 12 (3), 359–368.
Suo, Z., 1990. Singularities, interfaces and cracks in dissimilar anisotropic media. Proceedings of the Royal Society of London. Series A 427, 331–358.
Ting, T.C.T., 1986. Explicit solution and invariance of the singularities at an interface crack in anisotropic composites. International Journal of Solids and Structures 22, 965–983.
Ting, T.C.T., 1996. Anisotropic Elasticity: Theory and Applications. Oxford Science Publications, NY.
Wu, K.C., 1990. Stress intensity factor and energy release rate for interfacial cracks between dissimilar anisotropic materials. ASME Journal of Applied Mechanics 57, 882–886.